HHS Public Access

Author manuscript

Neuroimage. Author manuscript; available in PMC 2021 January 25.

Published in final edited form as:

Neuroimage. 2021 January 15; 225: 117517. doi:10.1016/j.neuroimage.2020.117517.

The macaque brain ONPRC18 template with combined gray and white matter labelmap for multimodal neuroimaging studies of Nonhuman Primates

Alison R. Weiss[a], **Zheng Liu**[a,b], **Xiaojie Wang**[a,b], **William A. Liguore**[a], **Christopher D. Kroenke**[a,b,c], **Jodi L. McBride**[a,c,d,*]

[a]Division of Neuroscience, Oregon National Primate Research Center, Beaverton, OR, USA, 97006

[b]Advanced Imaging Research Center, Oregon Health and Science University, Portland, OR, USA, 97239

[c]Department of Behavioral Neuroscience, Oregon Health and Science University, Portland OR, USA, 97239

[d]Department of Behavioral Neurology, Oregon Health and Science University, Portland OR, USA, 97239

Abstract

Macaques are the most common nonhuman primate (NHP) species used in neuroscience research. With the advancement of many neuroimaging techniques, new studies are beginning to apply multiple types of in vivo mag netic resonance imaging (MRI), such as structural imaging (sMRI) with T1 and T2 weighted contrasts alongside diffusion weighed (DW) imaging. In studies involving rhesus macaques, this approach can be used to better under stand micro-structural changes that occur during development, in various disease states or with normative aging. However, many of the available rhesus brain atlases have been designed for only one imaging modality, making it difficult to consistently define the same brain regions across multiple imaging modalities in the same subject. To address this, we created a brain atlas from 18 adult rhesus macaques that includes co-registered templates constructed from images frequently used to characterize macroscopic brain structure (T2/SPACE and T1/MP-RAGE), and a diffusion tensor imaging (DTI) template. The DTI template was up-sampled from 1 mm isotropic resolution to resolution match to the T1 and T2-weighted images (0.5 mm isotropic), and the parameter maps

*Corresponding author. mcbridej@ohsu.edu (J.L. McBride).

Credit Author Statement
Study Design: JLM, CK, ARW, ZL, XW
MR Image Acquisition: ARW, JLM, ZL, XW, CK
MR Image Processing: ZL, ZW, CK, ARW
Atlas ROI Delineation: ARW, WAL, JLM
Manuscript Preparation: ARW, JLM, CK, ZL, WAL, XW.

Declaration of Competing Interest
None.

Supplementary materials
Supplementary material associated with this article can be found, in the online version, at doi:10.1016/j.neuroimage.2020.117517.

were derived for FA, AD, RD and MD. The labelmap volumes delineate 57 gray matter regions of interest (ROIs; 36 cortical regions and 21 subcortical structures), as well as 74 white matter tracts. Importantly, the labelmap overlays both the structural and diffusion templates, enabling the same regions to be consistently identified across imaging modalities. A specialized condensed version of the labelmap ROIs are also included to further extend the usefulness of this tool for imaging data with lower spatial resolution, such as functional MRI (fMRI) or positron emission tomography (PET).

Keywords

Macaque; Brain atlas, DTI; MRI; Cortico-basal ganglia networks

1. Introduction

Nonhuman primates (NHPs) are valuable for translational neuroscience due to their relatively large and complex brain structure, their diverse behavioral repertoire, and their close phylogenic relationship with humans. Many neuroimaging studies with macaques require a species-specific magnetic resonance imaging (MRI) atlas to accurately delineate the anatomical boundaries of brain regions. Recent advances in neuroimaging techniques have spurred the generation of several NHP-specific MRI atlases and labelmaps, for example a T1-weighted MRI template by Rohlfing et al. (2012), a T2-weighted MRI template by Calabrese et al. (2015), and diffusion tensor imaging (DTI) templates by Zakszewski et al. (2014) and Adluru et al. (2012). Historically, atlases that have been designed for only one imaging modality represent a challenge for studies employing multiple neuroimaging modalities in the same study population. For such multi-modal neuroimaging studies, different templates can be applied separately to each scan modality. However, a limitation to this approach is that the corresponding label maps from each template may have slight-to-significant differences in boundary definitions, making it difficult to consistently define the same brain regions across multiple imaging modalities in the same subject.

To address this gap, we created a series of co-registered templates, including T1- and T2-weighted MRI as well as DTI. Regions of Interest (ROI) were defined to facilitate the investigation of cortico- and thalamo-basal ganglia circuitry and were informed by the boundaries described by Saleem & Logothetis (2007). This atlas builds on previous work from our group (INIA19 atlas, Rohlfing et al., 2012) using non-linear spatial normalization techniques (Avants et al., 2008; Yeo et al., 2008) to generate rhesus brain templates, and integrates high-resolution images from multiple image contrasts.

We have also made practical improvements in the labelmap to facilitate multi-modal neuroimaging studies. The INIA19 atlas (Rohlfing et al., 2012) applied NeuroMaps labels that were originally defined on a histological dataset (BrainInfo, 1991-present). However, in practice, we have found that both scan quality and individual variability in neuroanatomy impact the reliability and accuracy of registration-based segmentation approaches using highly-detailed and complex labelmaps with small ROIs. Here, we created a labelmap with fewer, more simplified ROIs that are better matched to the image resolution of in vivo MRI

and more tolerant of individual variation. To facilitate use of these templates for multimodal neuroimaging studies, the T1-weighted, T2-weighted, and diffusion-based images are registered to a common reference frame and labelmap. Moreover, to extend the usefulness of this tool for imaging data with lower spatial resolution, such as positron emission tomography (PET) or functional MRI (fMRI), a specialized condensed version of the labelmap ROIs was also generated.

2. Materials and methods

2.1. Subjects

Eighteen male (n = 6) and female (n = 12) adult rhesus macaques (ages 6–13) contributed to this study (Table 1). At the time the scans were collected, the animals were pair housed in standard indoor caging, maintained on a 7am/7pm light/dark cycle, given ad libitum access to water, and provided with monkey chow rations and fresh produce daily. The Institutional Animal Care and Use Committee (IACUC) approved all procedures used in this study, and all of the guidelines specified in the National Institutes of Health Guide for the Care and Use of Laboratory Animals were strictly followed.

To prevent motion artifacts and to ensure the safety of the animals, all monkeys were anesthetized for the duration of the scanning session. Anesthesia was initially induced with Ketamine HCl (15 mg/kg IM) and the animals were subsequently intubated to allow for maintenance of anesthesia by inhalation of 1–2% isoflurane gas vaporized in 100% oxygen. Animals were then placed in a head first, supine position on the scanner bed, and their heads were immobilized in the head coil with foam padding. Heart rate and blood oxygenation levels were observed and recorded by trained veterinary staff throughout the duration of the procedure. Upon completion of the scans, the animals were extubated, returned to their housing environment, and their recovery monitored closely for several hours.

2.2. MRI acquisition procedures

Images were acquired with a Siemens Prisma whole body 3T MRI system (Erlangen, Germany) using a 16-channel pediatric head rf coil. A vitamin E tablet taped to the right side of the head served as a fiducial marker. The images acquired included 3D T1-weighted magnetization-prepared rapid gradient-echo (MP-RAGE) (Mugler and Brookeman, 1990), 3D T2-weighted sampling perfection with application optimized contrasts using different flip angle evolution (SPACE) (Mugler et al., 2000), and diffusion tensor imaging (DTI). Detailed parameters for each scanning sequence are described in the sections that follow.

2.2.1. T1-weighted MP-RAGE—For 3D MP-RAGE imaging sequences, TE/TR/TI = 3.44/2600/913 ms, flip angle = 8°, voxel sizes were 0.5 mm isotropic and 224 slices were acquired. In-plane image sampling consisted of 320 by 320 data points in the phase-encoded and readout directions, respectively. Three MP-RAGE images were acquired in each imaging session and these were rigid-body registered to each other and averaged. Total MP-RAGE acquisition time was 31 min and 9 s.

2.2.2. T2-weighted SPACE—For 3D SPACE imaging sequences, TE/TR = 385/3200 ms, flip angle = 120°, voxel sizes and the field of view were the same as the 3D MP-RAGE images described above. Three SPACE images were acquired in each imaging session and these were rigid-body registered to each other and averaged. Total SPACE acquisition time was 29 min and 42 s.

2.2.3. Diffusion Tensor Imaging—Diffusion-weighted volumes were acquired using a monopoplar 2D diffusion-weighted, spin-echo planar imaging (EPI) sequence (TR/TE = 6700 ms/73 ms, GRAPPA factor = 2, echo train length = 52, resolution = 1 × 1 × 1 mm). Seven repetitions of 6 b0 volumes and 30 DW volumes with single b = 1000 s/mm^2 were acquired with the phase-encoding direction being anterior to posterior (A > P). To correct for the susceptibility induced distortions inherent to the EPI sequence, 1 b0 volume with opposite (P > A) phase encoding directions was also acquired. Total diffusion MRI acquisition time was 29 min and 39 s.

2.3. MR image preprocessing

A set of preprocessing operations was first applied to all acquired MR images to correct various types of artifacts and to extract brain masks. For T1-weighted and T2-weighted anatomic images (MP-RAGE and SPACE images), the artifacts such as motion and intensity inhomogeneity were corrected first, and then the brains were extracted for template construction. For DTI, the distortion of phase-encoding, motion and eddy current artifacts were corrected first, and subsequently the templates were constructed.

2.3.1. T1-weighted and T2-weighted anatomic image preprocessing—Both T1-weighted and T2-weighted images were preprocessed with identical procedures. In each imaging session, each of the three images were averaged after motion correction. For the motion correction, the first scanned image in each modality was selected as the reference, and other two images were registered to the reference using the rigid-body transformation. Next, the registered images and the reference image were averaged. All registration processing and averaging operations were carried out using ANTS (version 2.1; http://stnava.github.io/ANTs/) and FSL (version 5.0, http://fsl.fmrib.ox.ac.uk/fsl/fslwiki/). For all merged T1-weighed and T2-weighted images, intensity bias correction was performed using the “N4BiasFieldCorrection” tool in ANTS (Tustison et al., 2010). Next, T1- and T2-weighted head templates were constructed in the native coordinate using the “buildtemplateparallel.sh” tool in ANTS (Avants et al., 2010). Brain masks were drawn manually for head templates, and all bias field corrected subject T1- and T2-weighted images were non-linearly registered to the corresponding head templates. With the resulting registration parameters, the template brain masks were inversely mapped to each subject T1- and T2-weighted image spaces and the brains were extracted by the brain mask. The process of intensity bias correction for all brain images was repeated using the “N4BiasFieldCorrection” tool, in which the subject brain mask was used to limit the correction region to improve correction quality.

2.3.2. DTI preprocessing—All the DW volumes first underwent a de-noising step implemented in MATLAB (using a MATLAB script kindly provided by Dr. Sune Jespersen,

Aarhus University) (Veraart et al., 2016). Next, a susceptibility-induced off-resonance field (h) was calculated from the 6 pairs of b0 volumes with opposite phase-encoding direction using "topup," included in the FSL library (https://fsl.fmrib.ox.ac.uk/) (Andersson et al., 2003). An eddy current induced off-resonance field (e) and rigid-body transformations (r) between DW volumes to account for motion were estimated simultaneously using "eddy" (FSL). Finally, the 3 transformations (h, e, and r) were combined into one warp field to correct the de-noised DW volumes (Andersson and Sotiropoulos, 2016). "DTIFIT", another tool included in FSL library, was used to fit the de-noised, corrected b0s and DW volumes to a single tensor (DTI) model.

2.4. Multi-modal template construction and atlas creation

After preprocessing operations for the anatomic and DTI data were completed, population-based average brain templates were constructed. The T2-weighted template was constructed first as the reference for the other template constructions as described below.

2.4.1. T2-weighted template construction—All corrected T2-weighted brain images were initially aligned into a common space using a previously published T2 template (Calabrese et al., 2015) by rigid-body registration with the "antsRegistrationSyN.sh" tool. This reference frame was selected due to its high resolution and excellent tissue contrast, as well as its orientation in the standard 'MNI' space (Frey et al., 2011). This way, all transformed brain images were represented in a commonly used reference frame, possessing the same orientation and position. Next, an 'initial template' was generated from the resulting images using the "buildtemplateparallel.sh" tool (https://github.com/ANTsX/ANTs/blob/master/Scripts/buildtemplateparallel.sh) with one iteration and affine registration, using the default similarity metric (probability mapping). Then, the newly generated 'initial template' was used as the target and the template building command was re-run in four iterations using fully deformable registrations. The output was the final T2-weighted template.

2.4.2. T1-weighted template construction—The T2-weighted template was used as the reference for T1-weighted template construction. First, each corrected T1-weighted brain image was aligned to the corresponding T2-weighted brain image with a 12-parameter affine linear registration using mutual information as a cost function with the "antsRegistrantionSyN.sh" tool. Next, all T2-weighted brain images were b-spline non-linearly registered to the reference using the same software (ANTS version 2.1; http://stnava.github.io/ANTs/). Subsequently, with the resulting parameters, all aligned T1-weighted brain images were transformed to the T2-weighted brain template space. After averaging all transformed images, the T1-weighted brain template was obtained, which resided in the same reference frame as the T2-weighted template.

2.4.4. DTI Template—The diffusion tensor template was constructed from all 18 individuals and resampled with 0.5 mm isotropic voxel spacing using DTI-TK (https://www.nitrc.org/projects/dtitk), a tensor-based spatial normalization tool (Zhang et al., 2007). The procedure described in Adluru et al. (2012) was followed, in which tensor-based registrations were performed to generate a diffusion MRI template, which was subsequently

registered to the T2-weighted template. It has been demonstrated that templates created using tensor-based methods (i.e. DTI-TK) perform better than templates created using multimodal intrasubject registration methods (i.e. FA-T1 and B0-T2) (Adluru et al., 2012). For this reason, we adopted DTI-TK methods to generate the DTI template and then aligned the DTI template to the anatomical template space where multimodal registration operations were implemented only once, rather than to use intrasubject registrations to bring each subject's DTI images into the space of the T2 before template construction. Once completed, the diffusion tensor template was non-linearly mapped to the T2-weighted template. To achieve this, the b0 template was first non-linearly registered to the T2w template using "antsRegistrationSyn.sh", resulting in an affine transform and a warp field. Next, the diffusion tensor template was warped to the T2w space using the affine transform and the warp field generated from the previous step via "antsApplyTransforms" (with −e 2 option). Lastly, the affine transform and the warp field were combined into a single warp file which was used to reorient the diffusion tensors that were already in T2-weighted template space. The DTI-TK TVtool was then used to generate tensor derivatives (i.e. FA, MD, RD, and RGB color-coded FA images), which were subsequently reoriented with ITK-SNAP into RPI orientation to match the T1 and T2 templates.

2.5. Gray Matter (GM) Labelmap

The atlas of Saleem & Logothetis (2007) was used to define the boundaries of all cortical and subcortical Regions of Interest (ROIs) in the labelmap. ROIs were manually drawn on coronal sections of the T2 template by trained neuroanatomical experts (A.R.W., W.A.L., J.L.M.), using the 3D segmentation software ITK-SNAP (Yushkevich et al., 2006), and subsequently verified and edited in the axial and sagittal planes. Table 2 describes the anatomical boundaries used to delineate this labelmap, and Fig. 1 A provides 3-dimensional renderings of the ROIs. Additionally, to facilitate neuroimaging modalities where scans have lower spatial resolution, we created an auxiliary version of the GM labelmap with condensed cortical and sub-cortical ROIs (Table 2, Fig. 1 B).

2.6. Combined GM/WM labelmap

To provide segmentations of white matter (WM), we used a published diffusion tensor-based rhesus macaque atlas (Zakszewski et al., 2014) to identify and segment WM tracts on our templates. In order to combine these WM ROIs with our gray-matter (GM) ROIs into one consolidated labelmap, the WM labelmap was first applied to the FA template. To accomplish this, the FA template from Zakszewski et al. (2014) was nonlinearly registered to our FA template, and the resulting transformation applied to the WM labelmap. This process resulted in a number of voxels being redundantly labeled as GM and WM structures. Using ITK-snap, the overlapping voxels were manually categorized by a trained observer (A.R.W.), and then labelmaps combined using FSL commands. The cerebellum was defined in this atlas using only one consolidated ROI and so all overlapping WM ROIs in this region were assigned to part of the cerebellar ROI.

3. Results

We created a series of co-registered templates, including T1- and T2-weighted MRI as well as DTI, that are aligned with a set of labelmaps that define Regions of Interest (ROI) to facilitate the investigation of cortico- and thalamo-basal ganglia circuitry.

3.1. T1 and T2 templates and labelmaps

The anatomical T1 and T2 templates have identical native resolution (0.5 mm isotropic), and fields of view (60 mm by 79.5 mm by 50 mm). The templates are provided in neuroimaging informatics technology initiative (NIFTI) file format with all associated meta-data formatted to Brain Imaging Data Structure (BIDS) specifications (https://bids-specification.readthedocs.io/en/stable/), and have been uploaded to the NITRC data exchange under the name ONPRC.18 Multimodal Macaque MRI Atlas (https://www.nitrc.org/projects/onprc18_atlas (5.9 MB). Fig. 2 illustrates axial and coronal views of the T1 (Fig. 2 A,C) and T2 (Fig. 2 B,D) templates, respectively, at multiple levels throughout the brain, with the labelmap for one hemisphere provided as an overlay. Our labelmap defines 57 ROIs (36 cortical regions and 21 subcortical structures) using the atlas of Saleem & Logothetis (2007) as a guide. All of the labels are bilateral, except for the cerebellum. For reference, the anatomical boundaries are described in Table 2 and volumes of each ROI are reported in Table 3. Structures defined in this labelmap were chosen to facilitate the investigation of cortico-basal ganglia and thalamo-basal ganglia networks (Weiss et al., 2020a), and so less detailed segmentations are provided for regions such as the hindbrain and cerebellum. We also created a condensed version of the labelmap that is designed to be used for analyses where larger ROIs are useful, such as neuroimaging modalities with low spatial resolution like PET. This labelmap contains 17 ROIs (8 cortical regions and 9 subcortical structures), and is also described in Table 2. As in the more detailed labelmap, all labels in the condensed labelmap are bilateral except for the cerebellum.

3.2. Diffusion templates/labelmaps

The diffusion tensor template was constructed independently from 18 individual DW volumes and registered to the shared T1 and T2 reference frame. The tensor template, its derivatives such as FA, MD, AD, and RD, were also uploaded in NIFTI file format, along with and BIDS formatted meta-data, on NITRC (www.nitrc.org/projects/onprc18_atlas (74.7 MB). Fig. 3 A, C illustrates axial and coronal views of the FA template at multiple levels with the labelmap for one hemisphere provided as an overlay, and Fig. 3 B, D illustrates the RGB template as an overlay on the T1w template to highlight the spatial co-registration of the DTI and sMRI templates.

It is noteworthy that, because the template was built upon individual DW volumes with high resolution and good SNR, our FA template allows delineation of numerous cortical regions such as the dorsolateral prefrontal cortex and subcortical structures including those comprising the basal ganglia, in addition to white matter tracts throughout the brain. Therefore, to further broaden the applicability and take advantage of advancements in scanning technology, we created a labelmap that combines our GM segmentations (Fig. 4 A)

with segmentations of 74 WM tracts defined by a previously published macaque DTI atlas (Zakszewski et al., 2014) in Fig. 4 B. After co-registration of both labelmaps to the template-space, we identified a small number of voxels that were labeled in both the GM and WM labelmaps (Fig. 4 C, D). These voxels almost entirely fell along the boundaries between tissues (white matter-grey matter-CSF), (Fig. 4 E, F). The resolution of our template, compared to the template by Zakszewski et al. (2014), as well as differences in the age ranges of the animals in each template, required us to refine the boundaries of these ROIs to better match the anatomy. Table 3 describes all of the ROIs in this labelmap, and reports the volumes of each.

3.3. Example applications

We have included several examples of scans collected from individual macaques using a variety of neuroimaging modalities (sMRI, DTI, PET) with co-registered labelmaps (generated by AntsRegistration) to demonstrate potential applications for the ONPRC18 atlas. First, as part of an ongoing longitudinal study of cortico-basal ganglia circuitry in a rhesus macaque model of Huntington's disease, the atlas was applied to a DTI scan acquired from one of the individuals used to build the template after delivery of the mutant *HTT* gene to the caudate and putamen (Fig. 5 A). Close manual inspection of the overlays revealed satisfactory results of the registration and accurate anatomical segmentations. To further probe the versatility of this atlas, we also applied it to structural scans (T1w/T2w) that were collected from a juvenile, 3-year old Japanese macaque (Macaca fuscata) bearing a CLN7 gene mutation (macaque model of Batten disease) (Fig. 5 B,C) again with satisfactory registration despite differences in macaque species, age and disease model. Finally, we have applied our consolidated labelmap to 18F-Fallypride PET and 18F-FDG PET images (Fig. 5 D,E, respectively) collected from naïve adult rhesus macaques with satisfactory registration, despite the lower spatial resolution of these scans. Both PET scans were collected with co-aligned CT, and the atlas was registered using the CT skull as a reference and then moved into PET space. These examples demonstrate some of the potential applications for this atlas, and suggest that it can be a reliable and versatile tool for different kinds of macaque neuroimaging studies.

4. Discussion

We created a brain atlas designed to facilitate studies with macaques employing both structural MRI and diffusion weighed imaging (DWI). Template images of the structural contrasts (T2/SPACE, T1/MP-RAGE) and DWI parameter maps (FA, AD, MD, RD, RGB, b0) were constructed in the 0.5 mm isotropic voxel-spacing reference frame. The labelmap provides segmentations of 57 gray matter ROIs (36 cortical regions and 21 subcortical structures) as well as 74 white matter tracts, and overlays all of the structural and diffusion templates. A condensed version of the labelmap was also created, with 17 larger ROIs, to facilitate imaging modalities with lower spatial resolution, such as fMRI and PET.

The templates here were created from in vivo scans, rather than scans of post-mortem fixed-tissue as in Calabrese et al. (2015); Feng et al. (2017); Reveley et al. (2017). The obvious merit to the latter is the ability to employ very lengthy scanning sequences (that would be

inappropriate for use with living animals) in order to collect high quality data. Yet, the scanning acquisition parameters employed here resulted in templates with image quality approaching that of many post-mortem datasets. Furthermore, fixation techniques used on post-mortem tissue can alter brain volume and water content, or induce non-rigid distortions, and therefore represent an important limitation in the application of post-mortem atlases to *in vivo* neuroimaging, and to DWI in particular. In contrast, the templates included here provide references that were acquired from living subjects, a feature that was shown to result in good registration accuracy when applying this atlas to other *in vivo* neuroimaging studies with macaques.

The construction of the ONPRC18 templates contrasts from previously available NHP atlases in several additional significant ways. First, rather than mirroring across the midline to create a laterally symmetric template as in Calabrese et al. (2015); Moirano et al. (2019), the ONPRC18 atlas preserved bilateral asymmetry between hemispheres in order to better reflect variability among the macaque population, as suggested by Frey et al. (2011). Second, the demographic distribution of the population ONPRC18 animals is in the middle-age range for macaques (8.1 ± 2.2 years) and includes a higher proportion of females (66%) than many existent population-based templates for adult monkeys: *INIA19 template*: 8 ± 1.6 years, all males (Rohlfing et al., 2012); *NMT template*: 5.5y ± 1.7 years, 19% female (Seidlitz et al., 2018); *MNI template*: 'young adult', 20% female (Frey et al., 2011); *112RM-SL template*: 19.9 ± 6.9 years, 27% females (McLaren et al., 2009); versus *UNC-Wisconsin Neurodevelopment template: covers 0–3 years, 50% females* (Young et al., 2017); *UNC-Emory Infant template*: covers 0–12months, 50% females (Shi et al., 2016). These differences may be particularly relevant for brain regions and structures with a protracted development that extends beyond puberty or with vulnerability to advancing age, as well as for cross-sectional studies investigating sex differences. Third, new advances in SPACE pulse sequences have made it possible to collect high quality T2w images at identical resolution as T1w MPRAGE images, enabling either contrast to be used as a base anatomical dataset. Given that the T2w contrast provides a better reference for registration of DWI images than T1w (Adluru et al., 2012), the T2w template was selected as the primary reference for the construction of the ONPRC18 DTI- and T1w-templates. Finally, we noted that the contrast of the SPACE images offered some advantages for the anatomical delineation of deep-brain structures surrounded by white matter, such as the basal ganglia and thalamus, as compared to MPRAGE (see Fig. 2). Given the relevance of these structures to the circuitry defined in the labelmap, we assigned the T2w template as the primary reference.

The ONPRC18 labelmap includes gray matter ROIs that were hand drawn with reference to the cortical and subcortical boundaries described by Saleem and Logothetis (2007). Building on previous work from our group, the INIA19 atlas (Rohlfing et al., 2012), we have made several practical improvements in the labelmap to facilitate in vivo multi-modal neuroimaging studies. First, by manually defining every GM ROI on a template generated from 18 animals, rather than transferring boundaries from a series of 2D histological sections defined on a single animal, we avoided the limitations inherent to generating 3D digital atlases from 2D histological drawings, as described by Reveley et al. (2017); Moirano et al. (2019). This resulted in a labelmap that is well matched to the image resolution of in

vivo MRI and quite tolerant of individual variation in neuroanatomy, a feature clearly demonstrated in Fig. 5. Similarly, by manually drawing ROIs on both hemispheres of the template rather than mirroring the labelmap across the midline, the ability to describe individual variabilities in hemispheric asymmetry is improved. Lastly, the ONPRC18 labelmap defines many subcortical structures such as the caudate, putamen, internal and external globus pallidus, substantia nigra, as well as lateral and medial subdivisions of the thalamus. This feature contrasts with the widely used D99 labelmap that combines the caudate, putamen, and nucleus accumbens into one striatal ROI, (Reveley et al., 2017; Seidlitz et al., 2018). For these reasons, the ONPRC18 atlas will fill an unmet need for NHP imaging resources suitable for studies of cortico-basal ganglia and thalamo-basal ganglia circuitry.

To further increase the relevance of this tool for investigations of cortico- and thalamo-basal ganglia, we enhanced the ONPRC18 GM labelmap by combining it with segmentations of WM regions defined in a previously published macaque DTI atlas (Zakszewski et al., 2014). The combined GM-WM labelmap eliminates the need for researchers to apply separate GM and WM labelmaps to their datasets, thereby reducing the number of transformations needed since only one registration will be required. Additionally, the increased precision created by the elimination of overlaps in the labels, see Fig. 4, enables the same gray and white matter regions to be more consistently identified. This is a unique feature of this atlas, and it will improve the validity of comparisons between scans acquired from the same subject in different imaging modalities.

We are currently applying the ONPRC18 atlas to a longitudinal study querying cortico- and thalamo-basal ganglia circuitry in a newly developed AAV-mediated rhesus macaque model of Huntington’s disease (HD) (Weiss et al., 2020a). In this context, we have found preliminary evidence of DTI changes occurring early in disease progression that correlate with cognitive and motor disease phenotypes (Weiss et al., 2020b), progressive reduction in putamen volume (unpublished data), and have begun to quantify changes in regional dopamine receptor binding potentials with F18-Fallypride PET (unpublished data, Fig. 5). Additional work is also underway using this atlas to assess regional brain atrophy and alterations in white matter microstructure in a Japanese macaque model of Batten’s disease (McBride et al., 2018), demonstrating that these templates have wide versatility and can be successfully applied to other species and ages of macaques.

In summary, it is our hope that this new ONPRC18 atlas with corresponding label maps will serve as an updated resource for NHP researchers to facilitate investigations of macaque brain circuitry, for developing and characterizing models of neurological disease, assessing the pre-clinical safety and biodistribution of therapeutics and/or developing imaging signatures of disease as outcome measures for pre-clinical trials.

Supplementary Material

Refer to Web version on PubMed Central for supplementary material.

Acknowledgements

We sincerely thank the entire ONPRC Division of Comparative Medicine for the outstanding care of our rhesus macaques, with special acknowledgement of the efforts that Lauren Drew Martin, Theodore Hobbs, Michael Reusz, Brandy Dozier, Alona Kvitky, and Isabel Bernstein contributed to this work.

Funding Sources

This research was supported by funds from NIH/NINDS R01 NS099136, NIH/NINDS R24 NS104161 (NHP Resource for Preclinical Studies of Neurodegenerative Disease), NIH/NINDS F32 NS110149, NIH/NIAAA U24 AA025473, NIH P51 OD011092, the Bev Hartig Huntington's Disease Foundation and a grant from the M.J. Murdock Charitable Trust.

References

Adluru N, Zhang H, Fox AS, Shelton SE, Ennis CM, Bartosic AM, Oler JA, Tromp do PM, Zakszewski E, Gee JC, Kalin NH, Alexander AL, 2012 A diffusion tensor brain template for rhesus macaques. Neuroimage 59, 306–318. [PubMed: 21803162]

Andersson JL, Sotiropoulos SN, 2016 An integrated approach to correction for off-resonance effects and subject movement in diffusion MR imaging. Neuroimage 125, 1063–1078. [PubMed: 26481672]

Andersson JL, Skare S, Ashburner J, 2003 How to correct susceptibility distortions in spin-echo echo-planar images: application to diffusion tensor imaging. Neuroimage 20, 870–888. [PubMed: 14568458]

Avants BB, Epstein CL, Grossman M, Gee JC, 2008 Symmetric diffeomorphic image registration with cross-correlation: evaluating automated labeling of elderly and neurodegenerative brain. Med. Image Anal. 12, 26–41. [PubMed: 17659998]

Avants BB, Yushkevich P, Pluta J, Minkoff D, Korczykowski M, Detre J, Gee JC, 2010 The optimal template effect in hippocampus studies of diseased populations. Neuroimage 49, 2457–2466. [PubMed: 19818860]

BrainInfo, 1991-present In: National Primate Research Center. University of Washington.

Calabrese E, Badea A, Coe CL, Lubach GR, Shi Y, Styner MA, Johnson GA, 2015 A diffusion tensor MRI atlas of the postmortem rhesus macaque brain. Neuroimage 117, 408–416. [PubMed: 26037056]

Feng L, Jeon T, Yu Q, Ouyang M, Peng Q, Mishra V, Pletikos M, Sestan N, Miller MI, Mori S, Hsiao S, Liu S, Huang H, 2017 Population-averaged macaque brain atlas with high-resolution ex vivo DTI integrated into in vivo space. Brain Struct Funct 222, 4131–4147. [PubMed: 28634624]

Frey S, Pandya DN, Chakravarty MM, Bailey L, Petrides M, Collins DL, 2011 An MRI based average macaque monkey stereotaxic atlas and space (MNI monkey space). Neuroimage 55, 1435–1442. [PubMed: 21256229]

McBride JL, Neuringer M, Ferguson B, Kohama SG, Tagge IJ, Zweig RC, Renner LM, McGill TJ, Stoddard J, Peterson S, Su W, Sherman LS, Domire JS, Ducore RM, Colgin LM, Lewis AD, 2018 Discovery of a CLN7 model of Batten disease in non-human primates. Neurobiol Dis 119, 65–78. [PubMed: 30048804]

McLaren DG, Kosmatka KJ, Oakes TR, Kroenke CD, Kohama SG, Matochik JA, Ingram DK, Johnson SC, 2009 A population-average MRI-based atlas collection of the rhesus macaque. Neuroimage 45, 52–59. [PubMed: 19059346]

Moirano JM, Bezgin GY, Ahlers EO, Kotter R, Converse AK, 2019 Rhesus macaque brain atlas regions aligned to an MRI template. Neuroinformatics 17, 295–306. [PubMed: 30291569]

Mugler JP 3rd, Brookeman JR, 1990 Three-dimensional magnetization-prepared rapid gradient-echo imaging (3D MP RAGE). Magn. Reson. Med 15, 152–157. [PubMed: 2374495]

Mugler JP 3rd, Bao S, Mulkern RV, Guttmann CR, Robertson RL, Jolesz FA, Brookeman JR, 2000 Optimized single-slab three-dimensional spin-echo MR imaging of the brain. Radiology 216, 891–899. [PubMed: 10966728]

Reveley C, Gruslys A, Ye FQ, Glen D, Samaha J, B ER, Saad Z, A KS, Leopold DA, Saleem KS, 2017 Three-dimensional digital template atlas of the Macaque Brain. Cereb. Cortex 27, 4463–4477. [PubMed: 27566980]

Rohlfing T, Kroenke CD, Sullivan EV, Dubach MF, Bowden DM, Grant KA, Pfefferbaum A, 2012 The INIA19 template and neuromaps atlas for primate brain image parcellation and spatial normalization. Front. Neuroinform 6, 27. [PubMed: 23230398]

Saleem KS, Logothetis N, 2007 A combined MRI and histology atlas of the rhesus monkey brain in stereotaxic coordinates. MA: Academic, London; Burlington.

Seidlitz J, Sponheim C, Glen D, Ye FQ, Saleem KS, Leopold DA, Ungerleider L, Messinger A, 2018 A population MRI brain template and analysis tools for the macaque. Neuroimage 170, 121–131. [PubMed: 28461058]

Shi Y, Budin F, Yapuncich E, Rumple A, Young JT, Payne C, Zhang X, Hu X, Godfrey J, Howell B, Sanchez MM, Styner MA, 2016 UNC-Emory infant atlases for macaque brain image analysis: postnatal brain development through 12 months. Front. Neurosci 10, 617. [PubMed: 28119564]

Tustison NJ, Avants BB, Cook PA, Zheng Y, Egan A, Yushkevich PA, Gee JC, 2010 N4ITK: improved N3 bias correction. IEEE Trans. Med. Imaging 29, 1310–1320. [PubMed: 20378467]

Veraart J, Novikov DS, Christiaens D, Ades-Aron B, Sijbers J, Fieremans E, 2016 Denoising of diffusion MRI using random matrix theory. Neuroimage 142, 394–406. [PubMed: 27523449]

Weiss AR, Liguore WA, Domire JS, Button D, McBride JL, 2020a. Intra-striatal AAV2.retro administration leads to extensive retrograde transport in the rhesus macaque brain: implications for disease modeling and therapeutic development. Sci. Rep 10, 6970. [PubMed: 32332773]

Weiss AR, Brandon KR, Liguore WA, Liu Z, Wang X, Kroenke CD, McBride JL, 2020b AAV2.retro-mediated delivery of mHTT in the rhesus macaque caudate and putamen leads to the progressive development of dyskinesias, fine motor skill decline, and impairments in working memory. Annual CHDI Foundation Meeting.

Yeo BT, Sabuncu MR, Desikan R, Fischl B, Golland P, 2008 Effects of registration regularization and atlas sharpness on segmentation accuracy. Med Image Anal 12, 603–615. [PubMed: 18667352]

Young JT, Shi Y, Niethammer M, Grauer M, Coe CL, Lubach GR, Davis B, Budin F, Knickmeyer RC, Alexander AL, Styner MA, 2017 The UNC-Wisconsin Rhesus Macaque neurodevelopment database: a structural MRI and DTI database of early postnatal development. Front. Neurosci 11, 29. [PubMed: 28210206]

Yushkevich PA, Piven J, Hazlett HC, Smith RG, Ho S, Gee JC, Gerig G, 2006 User-guided 3D active contour segmentation of anatomical structures: significantly improved efficiency and reliability. Neuroimage 31, 1116–1128. [PubMed: 16545965]

Zakszewski E, Adluru N, Tromp do PM, Kalin N, Alexander AL, 2014 A diffusion-tensor-based white matter atlas for rhesus macaques. PLoS One 9, e107398. [PubMed: 25203614]

Zhang H, Avants BB, Yushkevich PA, Woo JH, Wang S, McCluskey LF, Elman LB, Melhem ER, Gee JC, 2007 High-dimensional spatial normalization of diffusion tensor images improves the detection of white matter differences: an example study using amyotrophic lateral sclerosis. IEEE Trans. Med. Imaging 26, 1585–1597. [PubMed: 18041273]

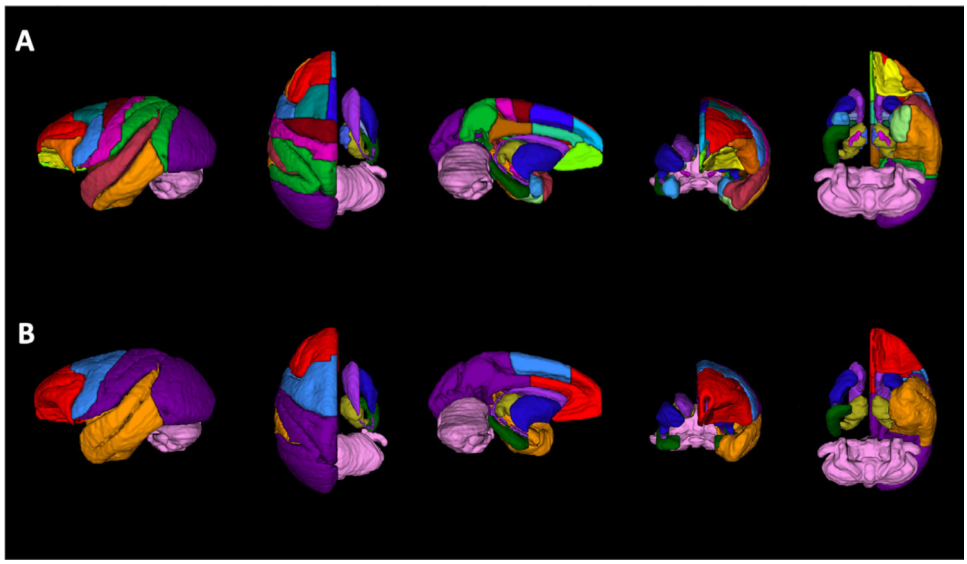

Fig. 1.

Rendering of labelmaps in 3-dimensions. (A) 3D-rendering of GM ROIs created using the 3D segmentation software ITK-SNAP, (Yushkevich et al., 2006). There are 57 cortical and subcortical ROIs defined in this labelmap. (B) Regions from the labelmap were subsequently categorized and combined to create a consolidated labelmap that defines 8 bilateral cortical ROIs and 9 subcortical structures, in order to facilitate neuroimaging modalities with low spatial resolution (i.e. rsfMRI, PET). To ease the visualization of subcortical structures, cortical regions in the right hemisphere were made transparent in this figure.

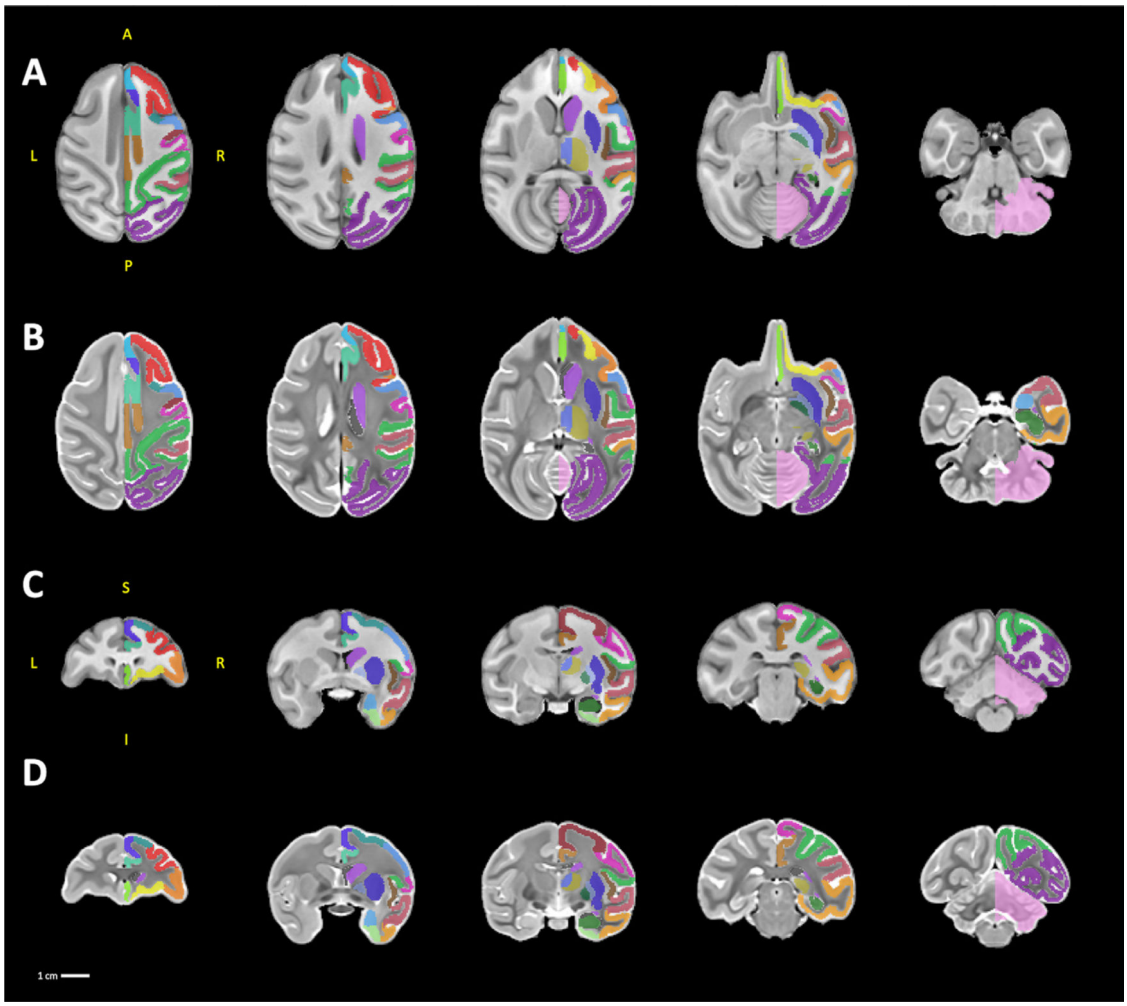

Fig. 2.

sMRI templates. A series of five axial and coronal sections displayed in neurological orientation through the T1 templates (A, C) and the T2 templates (B, D). For ease of viewing, the labelmap overlays are drawn only on the right hemisphere. *Abbreviations: A, anterior; I, inferior; L, left; P, posterior; R, right; S, superior.*

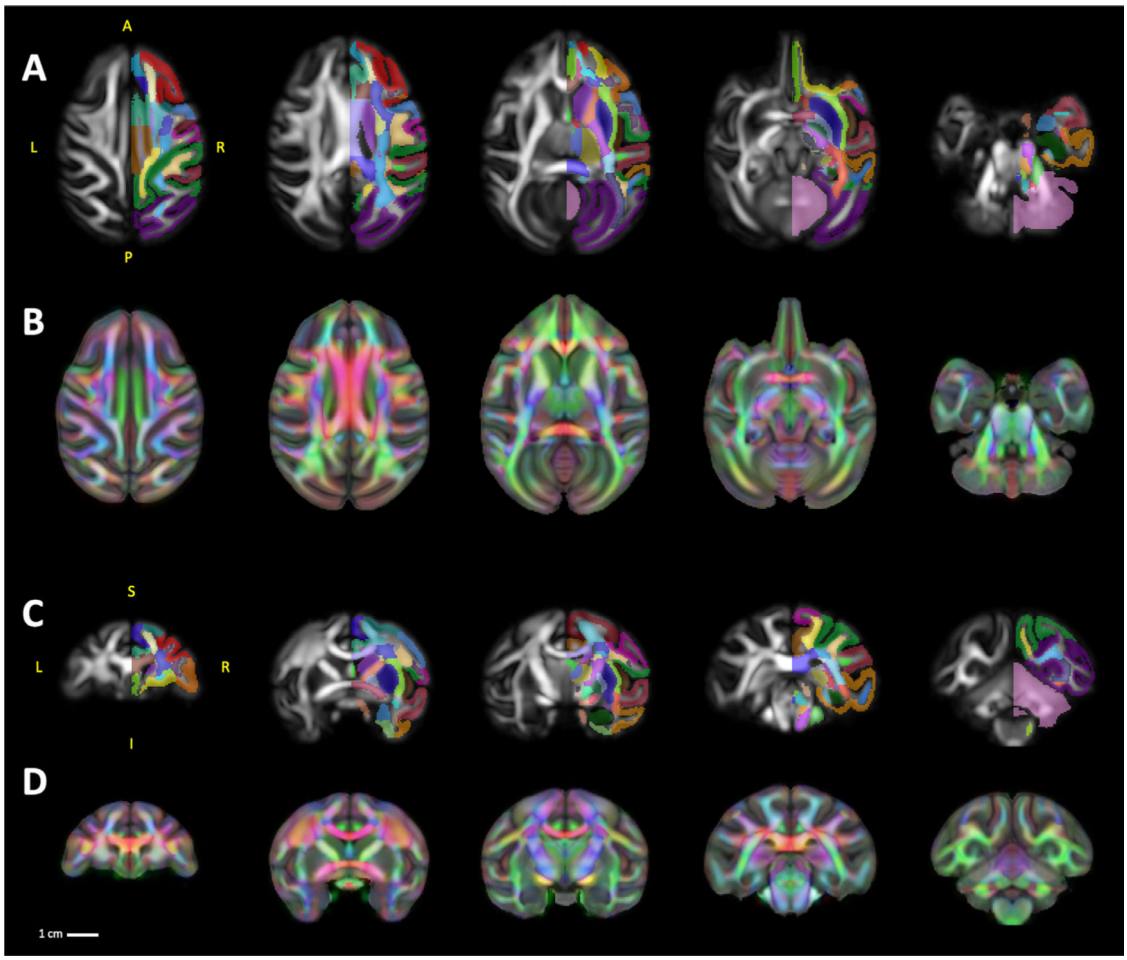

Fig. 3.

DTI Templates. A series of five axial and coronal sections displayed in neurological orientation through the FA template (A, C). For ease of viewing, the labelmap overlays are drawn only on the right hemisphere of the FA templates. To highlight the spatial co-registration of the DTI template with the sMRI templates (B, D) show visualization of RGB template as an overlay on the T1w template. *Abbreviations: A, anterior; I, inferior; L, left; P, posterior; R, right; S, superior.*

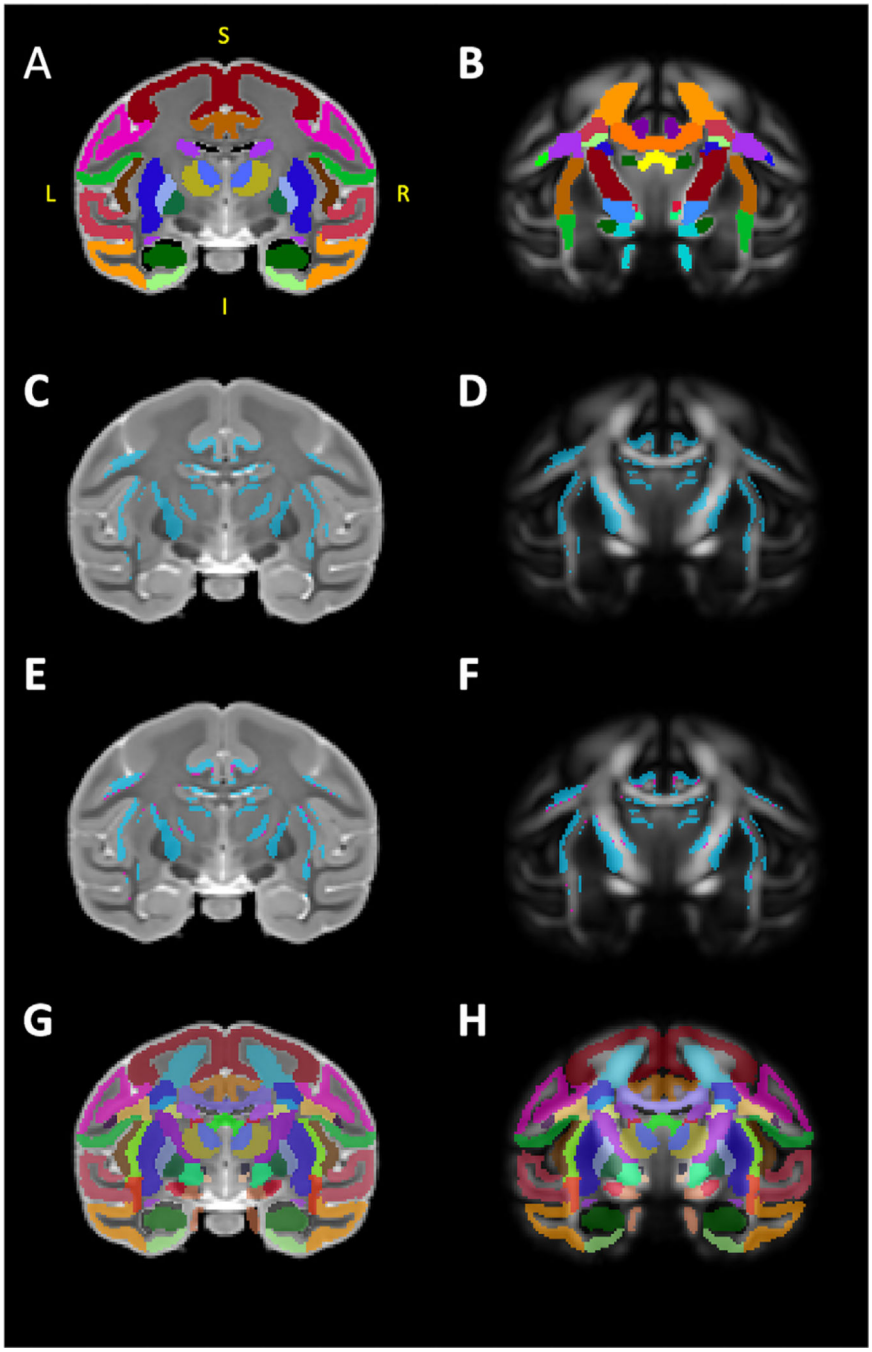

Fig. 4.

Combining gray and white matter labelmaps. (A) illustrates our gray matter (GM) labelmap overlaying the T2 template. We used a published diffusion tensor-based rhesus macaque atlas (Zakszewski et al., 2014) to identify and segment white matter tracts on our FA template, illustrated in (B). In order to combine these two labelmaps, using FSL tools, we first identified overlaps (i.e. double-labeled voxels) between the WM labelmap and our GM labelmap, these voxels are illustrated in blue in (C) and (D). ITK-SNAP was used to manually categorize these voxels as belonging to WM or GM, and the results of this

classification is illustrated in (E) and (F), with blue voxels categorized as GM and magenta voxels categorized as WM. Finally, the categorized voxels were reassigned to the appropriate GM/WM labelmap and ROI, and the two labelmaps were then consolidated into one. The results of this combination are illustrated in (G) and (H), overlaying the T2 and FA templates. *Abbreviations: I, inferior; L, left; P, posterior; R, right.*

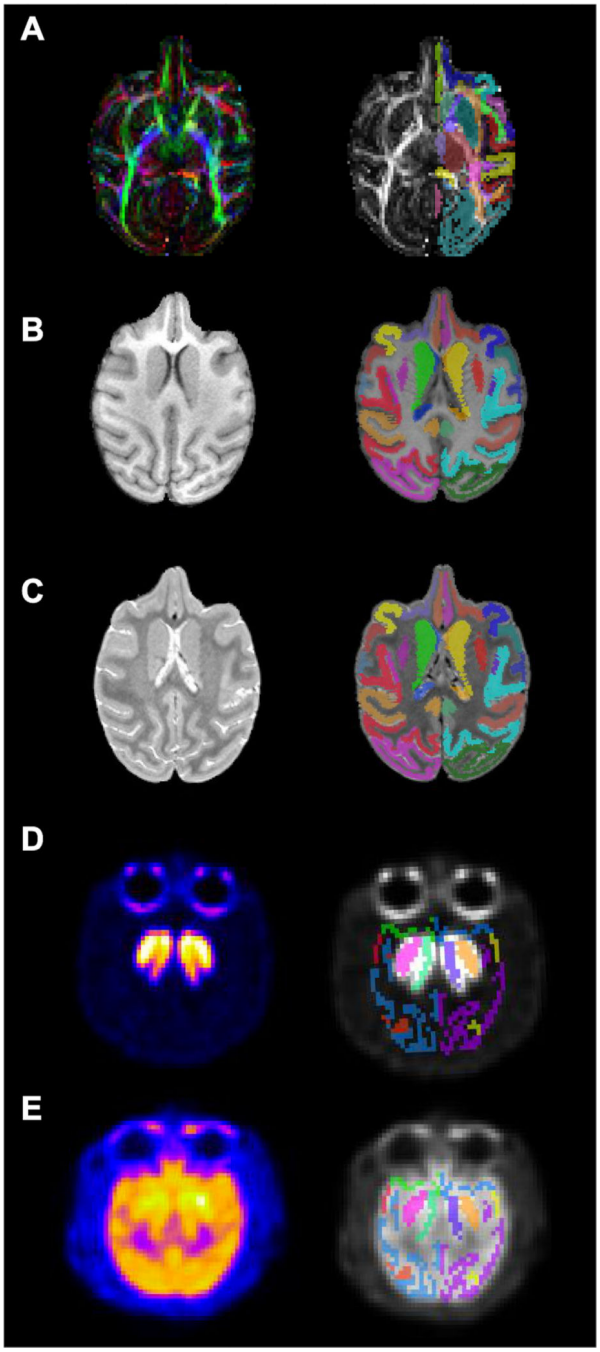

Fig. 5.

Example application of multimodal templates. A series of axial sections with co-registered labelmaps that illustrate applications of the ONPRC18 atlas to scans collected from individual macaques using a variety of neuroimaging contrasts and modalities (DTI, sMRI, PET). Label maps were generated by AntsRegistration software version 2.1; (http://stnava.github.io/ANTs/). (A) DTI scan acquired from one of the individuals in the template after intracranial administration of AAV-HTT (macaque model of Huntington's Disease) after intrac 6 months. (B, C) sMRI scans (T1w/T2w) that were collected from a juvenile

(3yo) Japanese macaque (Macaca fuscata) with a CLN7 mutation (macaque model of Batten disease). (D, E) 18F-Fallypride PET and 18F-FDG PET in a naïve female rhesus macaque. These examples demonstrate some of the potential applications for this atlas, and suggest that it can be a reliable and versatile tool for a wide variety of different kinds of macaque neuroimaging studies.

Table 1

Demographic information for study animals. Scans from 18 individual rhesus macaques contributed to these templates. At the time of the scans, the animals were 6–13 years old, and consisted of both males (n = 6) and females (n = 12).

Monkey	Sex	Age (years)	Weight (kg)
RH-1	F	13.47	9.9
RH-2	F	12.92	7.2
RH-3	F	12.21	7.4
RH-4	F	11.91	8.9
RH-5	F	11.76	6
RH-6	F	11.75	5.1
RH-7	F	10.03	5.8
RH-8	F	9.86	7.4
RH-9	F	8.92	8.3
RH-10	F	8.73	5.9
RH-11	F	8.69	6.5
RH-12	F	7.87	6.1
RH-13	M	9.97	9.6
RH-14	M	7.75	10
RH-15	M	7.62	11.8
RH-16	M	7.52	8.8
RH-17	M	7.01	10.9
RH-18	M	5.89	10.7

Table 2

Description of ROI anatomical boundaries in labelmaps. All regions were drawn by hand on the T2 template using the 3D segmentation software ITK-SNAP (Yushkevich et al., 2006). Cortical and subcortical ROIs were defined on coronal sections according to the atlas by Saleem & Logothetis (2007), and verified in the axial and sagittal planes. Regions from the labelmap were subsequently categorized and combined to create a consolidated labelmap that defines 8 bilateral cortical ROIs and 9 subcortical structures. Abbreviations: *1–2,* somatosensory areas 1 and 2; *3a/b,* somatosensory areas 3a and 3b; *7,* area 7 (all subdivisions); *8A,* area 8A; *8Bd,* area 8B, dorsal subdivision; *8Bm,* area 8B, medial subdivision; *8Bs,* area 8B in the arcuate sulcus; *9d,* area 9, dorsal subdivision; *9m,* area 9, medial subdivision; *10mrD,* area 10mr dorsal subdivision; *10mrM,* area 10mr medial subdivision; *10mrV,* area 10mr ventral subdivision; *11l,* area 11l; 11m, area 11m; *121,* area 12l; *12m,* area 12m; *12,* area 12 (all subdivisions); *13,* area 13 (all subdivisions); *14,* area 14 (all subdivisions); *23,* area 23 (all subdivisions); *24,* area 24 (all subdivisions); *25,* area 25; *29,* area 29 (retrosplenial cortex); *30,* area 30 (retrosplenial cortex); *31,* area 31; *32,* area 32; *35,* area 35; *36,* area 36 (all subdivisions); 44, area 44; 45, area 45; *46,* area 46 (all subdivisions); *AIP,* anterior intraparietal area; *AL,* anterior lateral, belt region of the auditory cortex; *CL,* caudal lateral, belt region of the auditory cortex; *cl,* central lateral nucleus; *CM,* caudomedial, belt region of the auditory cortex; *cnMD,* centromedian nucleus; *DP,* dorsal prelunate area; *EC,* entorhinal cortex (all subdivisions); *F1,* agranular frontal area F1; *F2,* agranular frontal area F2; *F3,* agranular frontal area F3; *F4*, agranular frontal area F4; *F5,* agranular frontal area F5; *F6,* agranular frontal area F6; *F7,* agranular frontal area F7; *FST,* floor of superior temporal area; *G,* gustatory cortex; *Ia,* agranular insula; *Iai,* intermediate agranular insula area; *Ial,* lateral agranular insula area; *Iam,* medial agranular insula area; *Iapl,* posterolateral agranular insula area; *Iapm,* posteromedial agranular insula area; *Id,* dysgranular insula; *Ig,* granular insula; *IPa,* area IPa (sts fundus); *LD,* lateral dorsal nucleus; *LIP,* lateral intraparietal area (all subdivisions); *LOP,* lateral occipital parietal area; *LP,* lateral posterior nucleus; *MD,* medial dorsal nucleus (all subdivisions); *MIP,* medial intraparietal area; *ML,* middle lateral, belt region of the auditory cortex; *MST,* medial superior temporal area; *MT,* middle temporal area; *Pcn,* paracentral nucleus; *Pf,* parafascicular nucleus; *PGa,* area PGa; *PI,* inferior pulvinar; *Pi*, parainsular area; *PIP*, posterior intraparietal area; *PL*, lateral pulvinar; *PM*, medial pulvinar; *PO*, parieto-occipital area; *PrCO*, precentral opercular area; *pulo*, pulvinar oralis nucleus; *R,* rostral, core region of the auditory cortex; *Ri,* retroinsula; *RM,* rostromedial, belt region of the auditory cortex; *RT,* rostrotemporal, core region of the auditory cortex; *RTL,* lateral rostrotemporal, belt region of the auditory cortex; *RTM,* medial rostrotemporal, belt region of the auditory cortex; *RTp*, rostrotemporal (polar); *SII*, secondary somatosensory area (S2); *STG*, superior temporal gyrus; *TAa*, area TAa (sts dorsal bank); *TE,* area TE (all subdivisions); *TEO,* area TEO; *TF*, area TF of the parahippocampal cortex; *TFO*, area TFO of the parahippocampal cortex, *TG,* area TG, temporal pole (all subdivisions); *TH,* area TH of the parahippocampal cortex; *TPO,* area TPO (sts dorsal bank); *Tpt,* temporoparietal area; *V1*, visual area 1 (primary visual cortex); *V2*, visual area 2; *V3,* visual area 3 (all subdivisions); *V4*, visual area 4 (all subdivisions); *VA*, ventral anterior nucleus; *VAmc*, ventral anterior nucleus, magnocellular division; *VIP*, ventral intraparietal area; *VL*, ventral lateral nucleus (all subdivisions); *VPI,* ventral posterior inferior nucleus; *VPLc,* ventral posterior lateral caudal nucleus; VPM, ventral posterior medial nucleus; *VPMpc,* ventral posterior medial nucleus, parvicellular division. Abbreviations from the atlas of Saleem and Logothetis (2007).

Atlas Region	Abbreviation	Label Number	Anatomical boundaries (as defined by Salem & Logothetis)	Consolidated Atlas Regions	Label Number
Dorsolateral Prefrontal	DLPFC-L	1	8A, 8Bd, 8Bs, 9d, 10mrD, 46	Frontal	1,2

Atlas Region	Abbreviation	Label Number	Anatomical boundaries (as defined by Salem & Logothetis)	Consolidated Atlas Regions	Label Number
Cortex	DLPFC-R	2			
Ventrolateral	VLPFC-L	3	12, 44, 45		
Prefrontal Cortex	VLPFC-R	4			
Orbital Prefrontal	OPFC-L	5	11, 13		
Cortex	OPFC-R	6			
Ventral Medial	VMPFC-L	7	10mrV, 14, 25, 32		
Prefrontal Cortex	VMPFC-R	8			
Dorsal Medial	DMPFC-L	9	8Bm, 9m, 10mrM,		
Prefrontal Cortex	DMPFC-R	10			
Anterior Cingulate	ACC-L	11	24		
Cortex	ACC-R	12			
Dorsal Premotor	DPMC-L	13	F2, F7	Motor	3,4
Cortex	DPMC-R	14			
Ventral Premotor	VPMC-L	15	F4, F5		
Cortex	VPMC-R	16			
Supplemental Motor	SMC-L	17	F3, F6		
Cortex	SMC-R	18			
Motor Cortex	MC-L	19	F1		
	MC-R	20			
Superior Temporal	STC-L	21	AL, CL, CM, ML, MST, PGa, R, RM, RT, RTL, RTM, RTp, STG, TAa, TEO, TG, TPO, Tpt	Temporal	5,6
Cortex	STC-R	22			
Inferior Temporal	ITC-L	23	FST, IPa, TE, TF, TFO, TH,		
Cortex	ITC-R	24			
Rhinal Cortex	RC-L	25	35, 36, EC		
	RC-R	26			
Insular Cortex	IC-L	27	Ia, Iai, Ial, Iam, Iapl, Iapm, Id, Ig, Pi, Ri,		
	IC-R	28			
Somatosensory Cortex	SSC-L	29	1–2, 3a/b, G, PrCO, SII,	Parieto-occipital	7,8
	SSC-R	30			
Parietal Cortex	PC-L	31	7, AIP, LIP, LOP, MIP, PIP, PO, VIP,		

Atlas Region	Abbreviation	Label Number	Anatomical boundaries (as defined by Salem & Logothetis)	Consolidated Atlas Regions	Label Number
	PC-R	32			
Posterior Cingulate	PCC-L	33	23, 29, 30, 31,		
Cortex	PCC-R	34			
Occipital Cortex	OCC-L	35	DP, MT, V1, V2, V3, V4,		
	OCC-R	36			
Caudate	CD-L	37		Caudate	9,10
	CD-R	38			
Putamen	PUT-L	39		Putamen	11,12
	PUT-R	40			
Lateral Thalamus	LatTh-L	41	cl, cnMD, LD, LP, Pf, PI, PL, PM, pulo, VA, VAmc, VL, VPI, VPlc, VPM, VPMpc	Thalamus	13, 14
	LatTh-R	42			
Medial Thalamus	MdTh-L	43	MD, Pcn		
	MdTh-R	44			
Hippocampus	HIPP-L	45	all subfields	Hippocampus	15, 16
	HIPP-R	46			
Amygdala	AMY-L	47	all nuclei	–	–
	AMY-R	48			
Substantia nigra	SN-L	49	pars compacta, pars reticulata	–	–
	SN-R	50			
Globus Pallidus	GPI-L	51		–	–
Internal	GPI-R	52			
Globus Pallidus	GPE-L	53		–	–
External	GPE-R	54			
Lat ventricles	LatV-L	55		–	–
	LatV-R	56			
Cerebellum	Cbm	57		Cerebellum	17

Table 3

Description of ROIs in Combined GM/WM labelmap. We used ROIs defined by a published diffusion tensor-based rhesus macaque atlas to identify and segment WM tracts on our FA template (Zakszewski et al., 2014). These WM ROIs were combined with our GM ROIs (described in Table 2) into one consolidated labelmap that is described by this table, as well as the volume (in mm^3) of each ROI in the labelmap.

Label Id	Structure	Abbreviation	Volume (mm^3)
1	Dorsolateral Prefrontal Cortex - Left	DLPFC_Left	986.625
2	Dorsolateral Prefrontal Cortex - Right	DLPFC_Right	985
3	Ventrolateral Prefrontal Cortex - Left	VLPFC_Left	377.75
4	Ventrolateral Prefrontal Cortex - Right	VLPFC_Right	371.75
5	Orbital Prefrontal Cortex - Left	OPFC_Left	370.5
6	Orbital Prefrontal Cortex - Right	OPFC_Right	376.125
7	Ventral Medial Prefrontal Cortex - Left	VMPFC_Left	335.125
8	Ventral Medial Prefrontal Cortex - Right	VMPFC_Right	326.125
9	Dorsal Medial Prefrontal Cortex - Left	DMPFC_Left	199.125
10	Dorsal Medial Prefrontal Cortex - Right	DMPFC_Right	197
11	Anterior Cingulate Cortex - Left	ACC_Left	341.75
12	Anterior Cingulate Cortex - Right	ACC_Right	337.75
13	Dorsal Premotor Cortex - Left	DPMC_Left	394.875
14	Dorsal Premotor Cortex - Right	DPMC_Right	394.875
15	Ventral Premotor Cortex - Left	VPMC_Left	444.375
16	Ventral Premotor Cortex - Right	VPMC_Right	437.75
17	Supplemental Motor Cortex - Left	SMC_Left	394.875
18	Supplemental Motor Cortex - Right	SMC_Right	389.75
19	Motor Cortex - Left	MC_Left	538.25
20	Motor Cortex - Right	MC_Right	557
21	Superior Temporal Cortex - Left	STC_Left	1632.12
22	Superior Temporal Cortex - Right	STC_Right	1643.38
23	Inferior Temporal Cortex - Left	ITC_Left	1391
24	Inferior Temporal Cortex - Right	ITC_Right	1373.88
25	Rhinal Cortex - Left	RC_Left	226.25
26	Rhinal Cortex - Right	RC_Right	225.5

Label Id	Structure	Abbreviation	Volume (mm^3)
27	Insular Cortex - Left	IC_Left	290.625
28	Insular Cortex - Right	IC_Right	288.5
29	Somatosensory Cortex - Left	SSC_Left	980.875
30	Somatosensory Cortex - Right	SSC_Right	971.75
31	Parietal Cortex - Left	PC_Left	1878.12
32	Parietal Cortex - Right	PC_Right	1857
33	Posterior Cingulate Cortex - Left	PCC_Left	381.75
34	Posterior Cingulate Cortex - Right	PCC_Right	376.75
35	Occipital Cortex - Left	OCC_Left	4205.62
36	Occipital Cortex - Right	OCC_Right	4216.88
37	Caudate - Left	CD_Left	511.625
38	Caudate - Right	CD_Right	511.875
39	Putamen - Left	PUT_Left	764.25
40	Putamen - Right	PUT_Right	754.625
41	Lateral Thalamus - Left	LatTh_Left	476.875
42	Lateral Thalamus - Right	LatTh_Right	476.125
43	Medial Thalamus - Left	MdTh_Left	132.75
44	Medial Thalamus - Right	MdTh_Right	134
45	Hippocampus - Left	HIPP_Left	400
46	Hippocampus - Right	HIPP_Right	400.375
47	Amygdala - Left	AMY_Left	198.125
48	Amygdala - Right	AMY_Right	198.875
49	Substantia nigra - Left	SN_Left	26.625
50	Substantia nigra - Right	SN_Right	26.5
51	Globus Pallidus Internal - Left	GPI_Left	70.125
52	Globus Pallidus Internal - Right	GPI_Right	71.25
53	Globus Pallidus External - Left	GPE_Left	153.625
54	Globus Pallidus External - Left	GPE_Right	154.625
55	Lateral ventricle - Left	LatVentricle_Left	314
56	Lateral ventricle - Right	LatVentricle_Right	328.625
57	Cerebellum	Cerebellum	6992.75

Label Id	Structure	Abbreviation	Volume (mm^3)
58	Middle Cerebellar Peduncle	MCP	564.75
59	Pontine Crossing Tract	PCT	80.375
60	Genu of Corpus Callosum	GCC	430.25
61	Body of Corpus Callosum	BCC	879.875
62	Splenium of Corpus Callosum	SCC	649
63	Fornix	FX	105.75
64	Anterior Commissure	AC	183
65	Pyramidal Tracts	PT	48.375
66	Corticospinal Tract - Right	CST-R	221
67	Corticospinal Tract - Left	CST-L	182.125
68	Medial Lemniscus - Right	ML-R	95.125
69	Medial Lemniscus - Left	ML-L	75.875
70	Inferior Cerebellar Peduncle - Right	ICP-R	40.875
71	Inferior Cerebellar Peduncle - Left	ICP-L	35.125
72	Superior Cerebellar Peduncle - Right	SCP-R	123.5
Label Id	Structure	Abbreviation	Volume (mm^3)
73	Superior Cerebellar Peduncle - Left	SCP-L	120
74	Cerebral Peduncle - Right	CP-R	164.75
75	Cerebral Peduncle - Left	CP-L	144.5
76	Anterior Limb of the Internal Capsule - Right	ALIC-R	269.375
77	Anterior Limb of the Internal Capsule - Left	ALIC-L	244.75
78	Posterior Limb of the Internal Capsule - Right	PLIC-R	351.5
79	Posterior Limb of the Internal Capsule - Left	PLIC-L	369.375
80	Retrolenticular Limb of the Internal Capsule - Right	RLIC-R	201.125
81	Retrolenticular Limb of the Internal Capsule - Left	RLIC-L	223.75
82	Anterior Corona Radiata - Right	ACR-R	372.125
83	Anterior Corona Radiata - Left	ACR-L	391.875
84	Superior Corona Radiata - Right	SCR-R	528.5
85	Superior Corona Radiata - Left	SCR-L	508.5
86	Posterior Corona Radiata - Right	PCR-R	441.25
87	Posterior Corona Radiata - Left	PCR-L	460.625

Label Id	Structure	Abbreviation	Volume (mm^3)
88	Posterior Thalamic Radiation - Right	PTR-R	484.125
89	Posterior Thalamic Radiation - Left	PTR-L	481.875
90	Sagittal Striatum - Right	SS-R	252.875
91	Sagittal Striatum - Left	SS-L	277
92	External Capsule - Right	EC-R	506.5
93	External Capsule - Left	EC-L	530.25
94	Superior Cingulum - Right	CgC-R	142.75
95	Superior Cingulum - Left	CgC-L	132.75
96	Perihippocampal Cingulum - Right	CgH-R	108.125
97	Perihippocampal Cingulum - Left	CgH-L	119.125
98	Stria Terminalus - Right	ST-R	219.75
99	Stria Terminalus - Left	ST-L	237.5
100	Superior Longitudinal Fasciculus - Right	SLF-R	487.25
101	Superior Longitudinal Fasciculus - Left	SLF-L	529
102	Superior Fronto-Occipital Fasciculus - Right	SFO-R	41.625
103	Superior Fronto-Occipital Fasciculus - Left	SFO-L	33.875
104	Uncinate Fasciculus - Right	UNC-R	125.5
105	Uncinate Fasciculus - Left	UNC-L	127.875
106	Tapetum - Right	TAP-R	43
107	Tapetum - Left	TAP-L	34
108	Dorsal Prefrontal WM - Right	DPF-R	231.625
109	Dorsal Prefrontal WM - Left	DPF-L	241
110	Ventral Prefrontal WM - Right	VPF-R	56.75
111	Ventral Prefrontal WM - Left	VPF-L	65.25
112	Dorsal Posterior Corona Radiata - Right	DPCR-R	483.125
113	Dorsal Posterior Corona Radiata - Left	DPCR-L	486
114	Medial Longitudinal Fasciculus - Right	MLF-R	38.375
115	Medial Longitudinal Fasciculus - Left	MLF-L	36.625
116	Central Tegmental - Right	CTG-R	70.625
117	Central Tegmental - Left	CTG-L	73.875
118	Inferior Frontal Gyrus WM - Right	IFG-WM-R	204.25

Label Id	Structure	Abbreviation	Volume (mm^3)
119	Inferior Frontal Gyrus WM - Left	IFG-WM-L	236.125
120	Superior Temporal Gyrus WM - Right	STG-WM-R	42.375
121	Superior Temporal Gyrus WM - Left	STG-WM-L	49.875
122	Middle Temporal Gyrus WM - Right	MTG-WM-R	174.375
123	Middle Temporal Gyrus WM - Left	MTG-WM-L	184.625
124	Adjacent Thalamus WM - Right	AT-WM-R	54.5
125	Adjacent Thalamus WM - Left	AT-WM-L	56.625
126	Adjacent Amygdala White Matter - Right	AA-WM-R	198.375
127	Adjacent Amygdala White Matter - Left	AA-WM-L	177.5
128	Midbrain White Matter WM - Right	MB-WM-R	102.375
129	Midbrain White Matter WM - Left	MB-WM-L	85.75